Geochemistry Geophysics Geosystems G3
AN ELECTRONIC JOURNAL OF THE EARTH SCIENCES
Published by AGU and the Geochemical Society

Article
Volume 7, Number 11
7 November 2006
Q11004, doi:10.1029/2005GC001216
ISSN: 1525-2027

Partitioning of strontium between calcite and fluid

R. I. Gabitov
Department of Earth and Environmental Sciences, Rensselaer Polytechnic Institute, 110 8th Street, JSC 1W19, Troy, New York 12180, USA

Now at Department of Geology and Geophysics, Woods Hole Oceanographic Institution, Woods Hole, Massachusetts 02543, USA (rgabitov@whoi.edu)

E. B. Watson
Department of Earth and Environmental Sciences, Rensselaer Polytechnic Institute, 110 8th Street, JSC 1W19, Troy, New York 12180, USA

[1] The Sr/Ca ratio of biogenic carbonate is widely used as a proxy for paleotemperature. This application is supported by empirical calibrations of Sr/Ca as a function of temperature, but it is also known that Sr uptake in calcite gauged by $K_d^{Sr} = \frac{(Sr/Ca)^{calcite}}{(Sr/Ca)^{solution}}$ is affected by other variables, including bulk precipitation rate (K_d^{Sr} increases with increasing precipitation rate). There are no data from controlled experiments specifically addressing the effect of radial growth rate of individual crystals on K_d^{Sr}. For this reason, we conducted two series of experiments to explore Sr partitioning at varying growth rates: (1) growth from a $CaCl_2$–NH_4Cl–$SrCl_2$ solution by diffusion of CO_2 from an ammonium carbonate source ("drift" experiments) and (2) "drip" precipitation of calcite on a substrate, using a steady flow of $CaCl_2$–$SrCl_2$ and Na_2CO_3 solutions, mixed just before passage through a tube and dripped onto a glass slide precoated with calcite ("cave-type" experiments). The growth rates of individual crystals were determined by periodic monitoring of crystal size through time or, roughly, by comparison of the final size with the duration of the experiment. Electron microprobe analyses across sectioned crystals grown in the drift experiments show that the concentration of Sr is high in the center (where radial growth rates are highest) and decreases systematically toward the edge. The center-to-edge drop in Sr concentration is a consequence of the slowing radial growth rate as individual crystals become larger. In general, high crystal growth rate (V) enhances Sr uptake in calcite due to a type of kinetic disequilibrium we refer to as "growth entrapment." The apparent K_d^{Sr} ranges from 0.12 to 0.35 as V increases from 0.01 nm/s to 1 μm/s at 25°C.

Components: 6826 words, 9 figures, 3 tables.

Keywords: calcite; partitioning; fluid; growth rate; strontium; temperature.

Index Terms: 1065 Geochemistry: Major and trace element geochemistry; 4825 Oceanography: Biological and Chemical: Geochemistry; 4875 Oceanography: Biological and Chemical: Trace elements (0489).

Received 9 December 2005; **Revised** 6 August 2006; **Accepted** 24 August 2006; **Published** 7 November 2006.

Gabitov, R. I., and E. B. Watson (2006), Partitioning of strontium between calcite and fluid, *Geochem. Geophys. Geosyst.*, *7*, Q11004, doi:10.1029/2005GC001216.

1. Introduction

[2] It is not unusual for the surface of a crystal in equilibrium with surrounding fluid to have a trace element composition different from that of the bulk crystal [*Paquette and Reeder*, 1995; *Reeder*, 1996; *Wasylenki et al.*, 2005a, 2005b; *Davis et al.*, 2004]. The growth entrapment model developed by Watson and coworkers [*Watson and Liang*, 1995; *Watson*, 1996, 2004] builds upon the above observation by evaluating the conditions under which a chemically anomalous surface gains expression in the composition of the bulk crystal. If the trace element of interest is enriched in the near-surface (relative to the equilibrium lattice) and if the local diffusivity (D_{surf}) of that element in the crystal is slow, then an anomalous surface composition may be completely or partially preserved by the growing crystal. This "entrapment" process can take place in any situation where the surface composition differs from that of the lattice, with the effectiveness depending mainly upon the competition between crystal growth rate (V) and the near-surface diffusivity. High growth rate and low diffusivity maximizes entrapment, so fast growing crystals may be particularly prone to this effect. This model addresses the behavior in the crystal only (in the near-surface region specifically), and does not consider diffusive boundary layer effects in the growth medium. Accordingly, it can be invoked in the simple form described above only for systems in which diffusion in the contacting fluid (or melt) is fast, as is this case for ions in seawater. A constant reservoir composition is also assumed that $C_i^{fluid} \neq f(x, t)$. The enhanced uptake of Sr^{2+} in calcite at high growth rates [*Lorens*, 1981; *Tesoriero and Pankow*, 1996; *Watson*, 2004; *Gabitov and Watson*, 2004] is readily explained by this entrapment mechanism. Sector zoning, known to occur in a wide variety of minerals (including calcite), is a definitive confirmation of growth entrapment disequilibrium for a special case in which the degree of surface enrichment is not the same for all crystal faces. For a given half-thickness (l) of the near-surface enriched layer, *Watson and Liang* [1995] predicted that if the dimensionless parameter $V \cdot l / D_{surf} > 0.5$, then occurrence of sector zoning is unavoidable in cases where the surface composition of adjacent growth faces is different. Growth entrapment may occur with uniform effectiveness on all growth faces when the surface compositions are all the same, in which case the lack of sectoral variation would mask the cause of disequilibrium.

[3] The precipitation rate of calcite is often quite high even at ambient conditions where diffusion in the near-surface region may be ineffective; consequently, sector zoning of trace elements in calcite is common [*Paquette and Reeder*, 1995; *Reeder*, 1996]. Diffusivities of Sr in the bulk calcite (D_{bulk}) at the temperature range from 435 to 800°C were evaluated by *Cherniak* [1997]. Extrapolating the diffusivity to 25°C using Cherniak's Arrhenius relationship yields $D_{bulk} = 1.53 \cdot 10^{-18}$ nm^2/s [*Watson*, 2004]. In contrast to D_{bulk}, data for D_{surf} are largely unknown. However, experimental data of *Stipp et al.* [1992] and modeling of Watson and coworkers suggest that D_{surf} of divalent metals might be as high as 10^{-3} and 10^{-1} nm^2/s, which is roughly 16 orders of magnitude faster than in the bulk lattice [*Stipp et al.*, 1992; *Watson*, 2004].

[4] Strontium in calcite is a valuable indicator of ocean chemistry and has seen extensive use in paleothermometry [e.g., *Elderfield et al.*, 1996, 2000, 2002; *Martin et al.*, 1999; *Andreasen and Delaney*, 2000; *Stoll et al.*, 2002a, 2002b]. Calcite is a widespread mineral common to marine sediments and hydrothermal rocks and also precipitates from aqueous solutions in limestone caves. The geometry of calcite growth surfaces plays an important role in the incorporation of impurities. *Paquette and Reeder* [1995] used differential interference contrast and cathodoluminescence microscopy to image the four vicinal surfaces of polygonized growth hillocks on calcite. *Davis et al.* [2004] confirmed using atomic force microscopy that the vicinal faces consistent of nonequivalent steps with different growth kinetic interpreted to arise form the different orientations of the carbonate groups at their edges. These two step types have nonequivalent step-edge geometries and kink-site structures because of differences in the orientation of the exposed carbonate groups. The combined data of *Paquette and Reeder* [1995], *Reeder* [1996], and *Davis et al.* [2004] suggest that the geometry of vicinal faces affects the bonding of divalent cations on the growing calcite surface.

[5] Cations larger than Ca^{2+}, e.g., Sr^{2+} and Ba^{2+}, form exclusively orthorhombic carbonates analogous to aragonite at ambient conditions. Therefore the coprecipitation of $SrCO_3$ (strontianite) is a favored mechanism of inclusion of Sr in calcite crystals. *Parkman et al.* [1998] studied Sr adsorption on the powdered calcite using SEM/EDS, and XAFS techniques. They found that very little Sr was removed from the solutions when the initial concentration is less than $3 \cdot 10^{-4}$ M, but at higher

Table 1. Composition of the Solutions in Mole per Liter[a]

	Solution	
	I	II
Ca^{2+}	$1.05 \cdot 10^{-2}$	$1.05 \cdot 10^{-2}$
NH_4^+	$4.83 \cdot 10^{-1}$	N/A
Cl^-	$5.04 \cdot 10^{-1}$	$5.04 \cdot 10^{-1}$
Na^+	N/A	$4.83 \cdot 10^{-1}$
Sr^{2+}	$2.57 \cdot 10^{-4}$	$2.57 \cdot 10^{-4}$
$I = 1/2 \Sigma m_i z_i^2$	$5.15 \cdot 10^{-1}$	$5.15 \cdot 10^{-1}$

[a] Notes: I is the ionic strength of solution, m_i is the concentration of the ion, and z_i is the charge of the ion.

concentrations, uptake increases linearly with initial Sr concentration. Thermodynamic arguments for strontianite precipitation from supersaturated solutions was confirmed by EXAFS spectroscopy, which yielded a Sr-O distance of 2.58 Å, very close to the value in pure Sr carbonate (2.59 Å). Examination of these samples by scanning electron microscopy and energy dispersive spectroscopy (SEM/EDS) suggested that at high Sr concentration in solution ($Sr > 3 \cdot 10^{-4}$ M) strontianite precipitates as a coating on the calcite surface. At lower initial Sr concentrations ($Sr < 3 \cdot 10^{-4}$ M), the Sr K-edge X-ray absorption near-edge spectrum (XANES) was different from those in strontianite but similar to the Ca K-edge spectrum in calcite, suggesting that Sr^{2+} substitutes for Ca^{2+} on the calcite surface rather than forming a discrete phase [*Parkman et al.*, 1998]. Given the knowledge that high Sr concentrations in the solution result in strontianite precipitation on the calcite surface, we grew our crystals from solutions (drift runs) in which Sr concentration was generally below $3 \cdot 10^{-4}$ M to avoid this situation.

[6] During crystal growth, $(Sr/Ca)^{calcite}$ is expected to be generally proportional to its ratio in the solution [*Lorens and Bender*, 1980; *Delaney et al.*, 1985]. Accordingly, the equilibrium partition coefficient we used in this study is defined as $K_d^{Sr} = \frac{(Sr/Ca)^{lattice}}{(Sr/Ca)^{solution}}$. Following *Watson and Liang* [1995] and *Watson* [1996], we also used a ratio called the surface enrichment factor (F), which is defined as the concentration, at equilibrium, of the element of interest in the near-surface region divided by concentration in the bulk lattice, that is $F = \frac{(Sr/Ca)^{surface}}{(Sr/Ca)^{lattice}}$. In future, the combination of bulk- and surface-analytical techniques may enable determination of F, but at present the magnitude of F is generally unknown.

[7] There exists a substantial data of Sr/Ca analyses of biogenic calcites. Ion microprobe analysis of natural foraminifera, for example, yields molar $Sr/Ca = 1.124 \cdot 10^{-6}$ (size of 420 μm) and $1.255 \cdot 10^{-6}$ (size of 620 μm) [*Allison and Austin*, 2003]. Assuming, Sr/Ca of seawater equals $8.54 \cdot 10^{-3}$, *Elderfield et al.* [1996] showed that mean partition coefficient increases with increasing size of forams. They observed a significant variation in K_d from 0.183 to 0.206 in the forams with the size of 250–300 μm. However, with increasing size the values of K_d showed less deviation from the average, thus $K_d^{Sr} = 0.197$–0.203 when the forams exceed 925 μm. Experimental studies with biogenic calcite yielded the following values of K_d^{Sr}: 0.16 ± 0.02 from experiments with foraminiferal calcite (*Globigerinoides sacculifer*) at 30°C [*Delaney et al.*, 1985], 0.13 ± 0.01 with molluscs (*Mytilus edulis*) at 23 ± 1°C [*Lorens and Bender*, 1980]. *Lea et al.* [1999] observed that foraminiferal Sr/Ca increases by 1% with increasing temperature by 1°C over the range $T = 16$–27°C. Experimental data [*Katz et al.*, 1972; *Gabitov and Watson*, 2004] and thermodynamic considerations ($\Delta H^0 = RT \ln K_d < 0$) suggest that K_d^{Sr} decreases with increasing temperature (5–97°C). It thus seems possible that uptake of Sr by foraminifera reported in the study of *Lea et al.* [1999] may be controlled by kinetic or biological factors. Previous studies show that K_d^{Sr} is a strong function of calcite growth rate [*Lorens*, 1981; *Tesoriero and Pankow*, 1996; *Stoll and Schrag*, 2000]. The partition coefficient increases from 0.02 to 0.14 as the precipitation rate increases from 3 to 160 nmol/(mg·min).

[8] In the previous studies noted above, Sr/Ca determinations were made on bulk calcite precipitates. No information was obtained on Sr variations within individual crystals, and the growth rate could only be estimated on the basis of the bulk mass precipitation rate. Our approach differs in that we examined single crystals whose growth rates could be reasonably well characterized. We applied two different techniques to determine the K_d^{Sr} at the wide range of calcite growth rates: from 0.03 nm/s to 1 μm/s. The range of growth rates we used overlaps with those of natural marine carbonates.

[9] Our partitioning data from drift experiments can be applied to the calcite–seawater systems with correction for the difference in activity coefficients of Ca_{aq}^{2+} and Sr_{aq}^{2+}. The 2nd approximation of the Debye–Huckel equation reveals the activity coefficients are the same for Sr and Ca and equal to

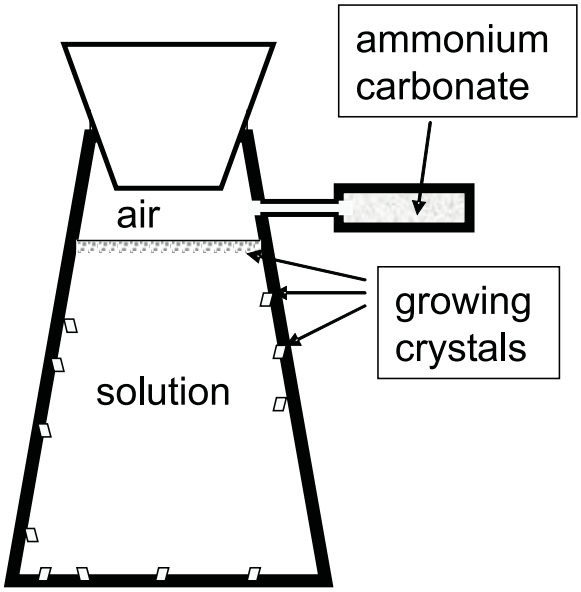

Figure 1. Schematic diagram of the experimental apparatus used for the drift method.

0.21 in our experimental solutions (drift experiment) and to 0.19 in seawater at 25°C.

2. Experimental and Analytical Details

2.1. Drift Experiment

[10] We conducted these experiments in a manner similar to that described by *Gruzensky* [1967] and *Paquette and Reeder* [1995]. Calcite crystals were precipitated from $CaCl_2$-NH_4Cl (or NaCl) $CaCO_3$-saturated solutions (see Table 1) in response to the diffusive flux of CO_2 from decomposition of ammonium carbonate [$(NH_4)_2CO_3$] at temperatures ranging from 5 to 97°C and 1 atm. Solutions doped with $SrCl_2$ were transferred into a Pyrex beaker or Nalgene container connected to a glass vial containing ammonium carbonate (Figure 1).

[11] At ambient temperature ammonium carbonate crystals decompose according to the reaction

$$(NH_4)_2CO_3 \rightarrow 2NH_{3(g)} + CO_{2(g)} + H_2O_{(g)} \qquad (1)$$

Gaseous species NH_3 and CO_2 dissolve and diffuse into the $CaCl_2$-NH_4Cl solution in which they dissociate following the equilibrium reaction schemes [see *Lemarchand et al.*, 2004]. These reactions result in an increase of pH and total alkalinity of the solution yielding an increase in the saturation state (Ω) with respect to calcite. After onset of crystallization the solutions remained at a nearly constant pH [*Lemarchand et al.*, 2004]. These authors mentioned that NH_3/NH_4^+ system buffers pH during the precipitation of calcite. The amount of Ca in the final solution was calculated from the mass balance method in runs D-1 and D-2 and analyzed by atomic absorption (AA) spectrometry in run D-3 (see Table 2). The concentration of DIC was determined by gas chromatography. However, we did not measure alkalinity in the solution, so the degree of saturation state in our system remains unclear. *Paquette and Reeder* [1995] estimated the value of Ω to be 15 in a similar experiment with the same solution composition as our runs D-1 and D-2. Unfortunately, almost all solutions were inadvertently discarded, thus precluding atomic absorption analyses of the final composition in most of the drift runs.

[12] The parameters of the runs are listed in Table 3. The temperature was maintained as follows: by refrigerator (T = 5 ± 2°C), at room conditions (T = 25 ± 5°C), in a water bath (T = 55 and 65 ± 1°C), and on a hot plate (T = 97 ± 3°C). The largest temperature gradient was observed in the hot plate set up: the solution at the bottom of the flask was 1°C cooler than at the surface (at a distance of ~12 cm). Calcite crystals (size of 0.1–2 mm) nucleated at the surface of the solution and on the substrate provided by the container walls. The pH of the solutions was measured at room temperature using an ORION gel-filled combination electrode (relative accuracy ±0.02) connected to an ORION meter (model 210A). The pH values were obtained a few days after the end of the experiment from solutions that had been stored in sealed containers with 10–15 vol% of air. Our values (7.9 ± 0.1) were slightly higher than those measured by *Paquette and Reeder* [1995, Table 1] for a similar

Table 2. Calculated and Analyzed Solution Concentrations in Mole Per Liter[a]

Run	$Ca_{in} \times 10^{-2}$	$Sr_{in} \times 10^{-4}$	$Ca_{fin} \times 10^{-2}$ Calculated	$Sr_{fin} \times 10^{-4}$ Calculated	$Ca_{fin} \times 10^{-3}$ Analyzed	DIC $\times 10^{-3}$ Analyzed
D-1(Sr)	1.05	2.57	0.664	2.32	N/A	3.46
D-2(Sr)	1.05	2.57	0.484	2.39	N/A	7.19
D-3(Sr)	1.05	2.57	N/A	N/A	0.029	11.73

[a] Initial concentrations (in) compared with final values (fin) calculated from mass balance and measured by atomic absorption spectroscopy.

Table 3. Summary of Partitioning Data[a]

run	s.n.	Vol, ml	T°C	t, days	K_d Mean	K_d Maximum	K_d Minimum
D-1	I	35	5 ± 2	294	0.21	0.25	0.15
D-2	I	35	25 ± 5	294	0.24	0.35	0.12
D-3	I	35	55 ± 1	90	0.14	0.16	0.09
D-4	I	35	65 ± 1	10	0.12	0.20	0.06
D-5	I	35	97 ± 3	6	0.08	0.10	0.07
D-6	II	35	97 ± 3	6	0.11	0.13	0.08
C-1[b]		<1	25 ± 2	2.78	0.041	0.057	0.033

[a] D, drift experiment; C, cave-type experiment; s.n., solution number (from Table 1); Vol, volume of the growth container.
[b] In the cave-type experiment the ratio of Sr/Ca in the growth medium is independent of time.

composition of solution. In their study, pH was monitored more frequently, and showed an increase from 5.6 ± 0.1 to 7.7 ± 0.2 over the first two days until the solution reached saturation state. The pH then decreased to 7.3 ± 0.2 with the onset of nucleation and rapid crystal growth. After this point, the solution remained at a nearly constant pH [*Paquette and Reeder*, 1995].

2.2. Cave-Type Experiment

[13] In these experiments we used a technique similar to that described by *Huang and Fairchild* [2001]. Precipitation occurred on a glass plate (precoated with calcite of 1–5 μm in size), using a steady flow of $4.2\cdot10^{-3}$ M $CaCl_2$ + $2\cdot10^{-3}$ M $SrCl_2$ and $4.2\cdot10^{-3}$ M Na_2CO_3. These solutions were premixed at I = 0.01 just before passage through a tube set up to drip the solution onto a marked area of the plate at 25 ± 2°C (Figure 2). A dual syringe pump was configured for an injection rate of 0.023 ml/min, equivalent to $9.7\cdot10^{-8}$ mol of precipitated calcite per minute. Crystals grew to size of 40–60 μm in 86 hours. Longer experiments did not yield appreciably larger crystals. Humidity in the outer glass container (see Figure 2) was controlled by maintaining water in the container bottom.

2.3. Estimation of Growth Rate

[14] Crystals from the drift-type experiments were analyzed along directions perpendicular and parallel to the center of the wall surface on which they nucleated. We considered that the center of the crystal face in contact with the flask surface was the initial nucleus (Figure 3). Assuming a hemispherical shape and a constant volumetric precipitation rate (V^{precip}) we can calculate the radial growth rate (V) at each point from the center to the surface of the hemisphere $V = (dr) / (dt) = 0.261\cdot\left[\left(V^{precip}\right)^{1/3}\right]/t^{2/3}$ using the following relationship $Volume = V^{precip} \cdot t = \frac{2}{3}\pi r^3$, where r and t are the crystal radius and time, respectively. Hence the radial growth rate decreases with increasing time. The same calculations were performed for the rhombic shape of the crystal. The

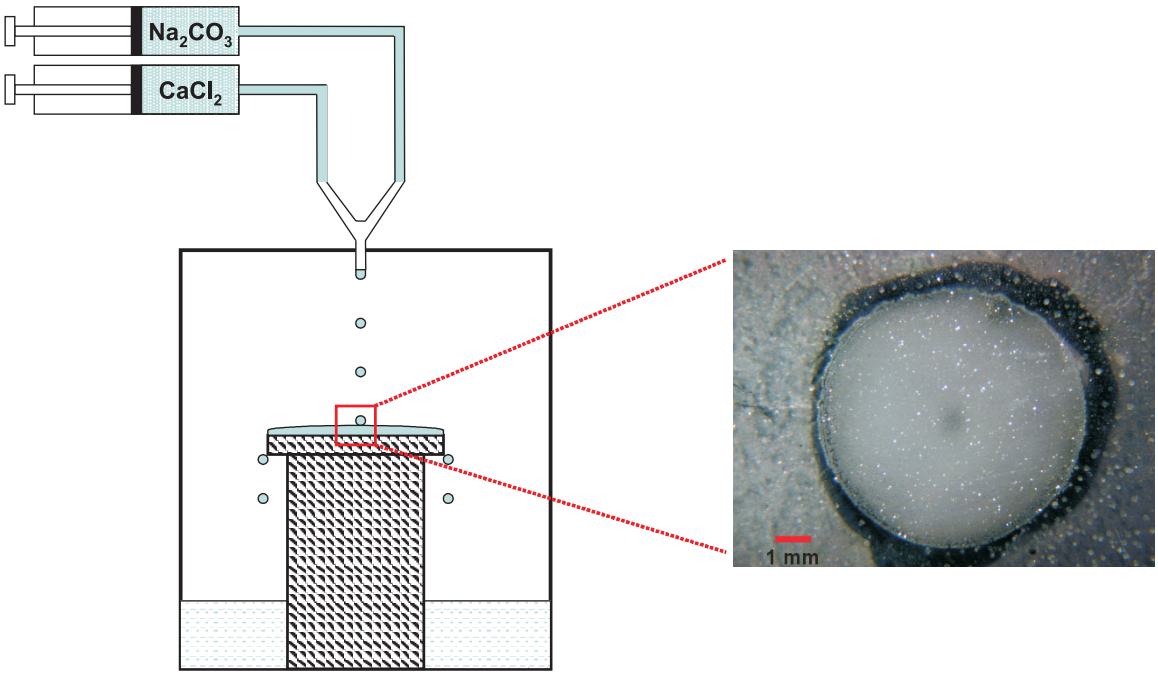

Figure 2. Schematic diagram of experimental apparatus used for the cave-type method.

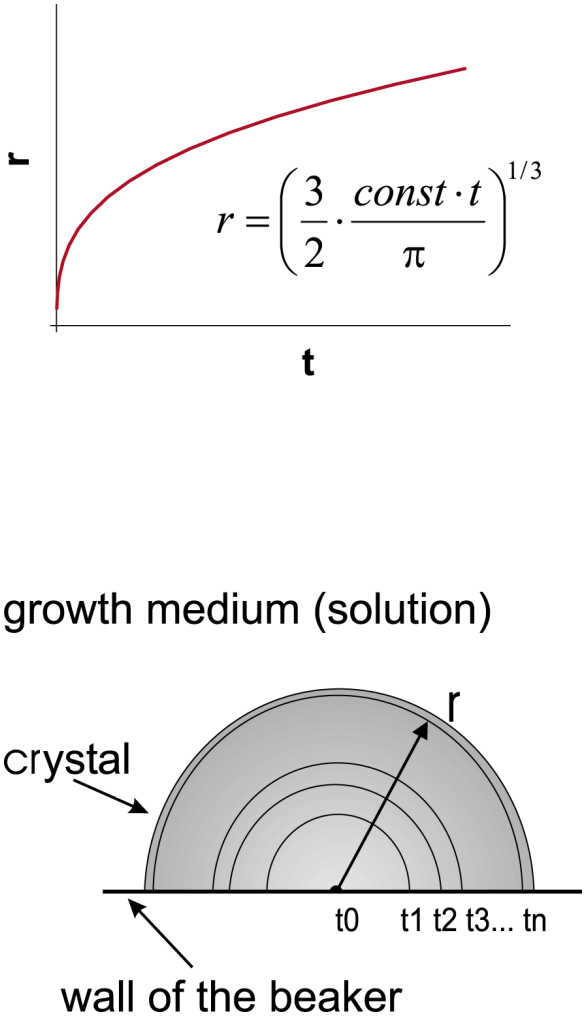

Figure 3. Method of estimating growth rate in drift experiment. The radial growth rate decreases with increasing of time and radius of the crystal.

values we obtained for log(*V*, nm/s) were shifted downward by 0.24 units relative to those for the hemispherical shape. We understand that the assumption of a constant rate of volumetric crystallization may not be strictly valid because of Ca and Ω of the fluid decreased over the course of the experiment slowing down the calcite precipitation rate. However, the decrease of the precipitation rate with time complements the decrease of the linear growth rate from the center to the edge of the crystals.

[15] In the cave-type experiment we monitored the size of the crystals as a function of time in the marked area (the center of the spot with the size of ≈300 μm) where the $CaCl_2$-Na_2CO_3 solution dripped down. We estimated the growth rate both by direct monitoring of the size of three selected crystals during the experiment, and by measuring the crystal thicknesses from back-scattered electron images upon experiment completion. The fragment of the glass plate precoated with calcite was temporarily removed from the experimental setup 21 hours (t_1) after the start of the run. The three crystals in the center of the marked area were photographed and quickly returned to the drip stage (this procedure required ~3 minutes). At the end of the run (86 hours = t_2) the same crystals were photographed again. Comparison of their sizes allowed us to determine growth rate at two time intervals $t_1 - t_0$ and $t_2 - t_1$. The second method of estimation of the growth rate in the cave-type experiment is described in the next paragraph.

[16] The silica glass plate with precipitated calcite was mounted into epoxy in a position slightly tilted relative to the exposed (polished) surface, forming an angle of α ($\alpha \approx 0.05$ degrees) (Figure 4). We calculated α using a distance interval from the crystal-glass boundary (zone where calcite was polished out completely) to the point where no Si was detected by EMP in a calcite analysis, which implies a calcite thickness of about 2.5 μm based on the calculated X-ray generation depth. Then the thickness of each measured crystal was determined by the simple geometrical relationship: $h = d \cdot tg\alpha$, where h is the thickness and d is the distance from the crystal-glass boundary. The range of growth rates estimated using this technique covers those determined by the size monitoring method described in the previous paragraph.

[17] Bulk precipitation rates from previous studies were converted to linear growth rates for comparison with this work. The rate units of nmol/($m^2 \cdot$ hr) and nmol/(cm^2·min) from *Mucci and Morse* [1983] and *Huang and Fairchild* [2001] were converted into linear ones using the molar volume of calcite (36.93 cm^3/mol). The units of nmol/(mg·min) from *Lorens* [1981] and *Tesoriero and Pankow* [1996] were translated into nm/s by using of the calcite molar volume and the specific surface areas of the seed crystals from their experiments (0.8 and 0.6 m^2/g).

2.4. Electron Microprobe (EMP) Analyses

[18] Calcite crystals recovered from the various experiments were rinsed with calcite-saturated H_2O (except run D-3) and then dried at 105°C. After mounting in epoxy the crystals were polished with fine Al_2O_3 powder (down to 1 μm in size), and examined using a wavelength dispersive elec-

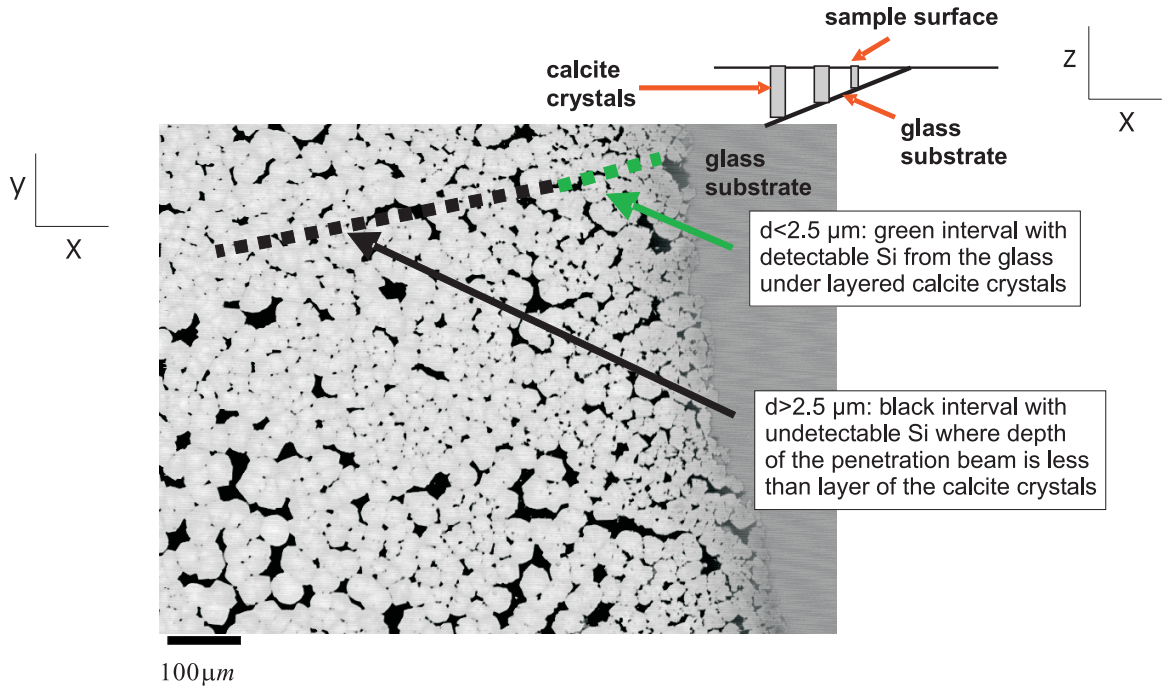

Figure 4. Method of estimation of growth rate in the cave-type experiment. See text for explanations. The crystal image is in the x-y plane. The inset shows (x-z plane) the change of the crystal thicknesses within the distance from the boundary where crystals were completely polished out.

tron microprobe (JEOL 733 Superprobe). Analyses were performed at following conditions: 15–17 nA sample current, 15 kV accelerating potential, 10–20 μm spot for 60–180 s of counting time. Calcite and strontianite were used as standards for Ca and Sr analyses, respectively.

2.5. Atomic Absorption (AA) and Gas Chromatography (GC) Analyses

[19] Filtered solutions from the crystallization experiments were analyzed for Ca with a Perkin-Elmer atomic absorption spectrometer (model 1100B) using a Fisher Scientific Ca/Mg hollow cathode lamp. Measurements were performed at a wavelength of 422.7 nm, slit band width of 0.7 nm, and acetylene/air fuel/oxidant. Fisher Scientific reference solutions of 1000 mg/L were used for preparing standard solutions of Ca. Dilution of the reference solution in 2% HNO_3 yielded three different standards: 5.0, 2.5, and 1.0 μg/mL of Ca. The standard deviation of measured samples from calibration line in AA analyses is equal to $5{\cdot}10^{-6}$ M.

[20] Filtered solutions from a crystallization experiments were analyzed for dissolved inorganic carbon (DIC) using a gas chromatograph (Table 2). Standard solutions were prepared by dissolution of Na_2CO_3 (Fisher Scientific 99.6%) in water at concentrations of 1.0, 2.5, 3.0, 4.0, 5.0, and 10.0 mM. Samples were mixed with dilute H_2SO_4 (2%) in a syringe and shaken to release CO_2. The resulting gas phase was then injected into the vaporizing chamber.

3. Results and Discussion

[21] Electron microprobe analyses yielded a range of Sr content (0.13–0.35 wt%) as a function of position in the crystals. Two perpendicular EMP profiles through calcite crystals from the polished "half-crystal" section of run D-2 are shown on Figure 5a. The profile obtained moving directly away from the center of the crystal-beaker boundary is marked as AB. The drop in the concentration ~150 μm from point A (Figure 5b) corresponds to the boundary (point A′) between light and dark areas on the back-scattered electron (BSE) image. We could not discern the BSE brightness transition corresponding to the next drop of Sr/Ca at a distance of 1000 μm. The profile parallel to the crystal-beaker boundary is marked as CD. The average shape of the concentration profile shows a monotonic decrease in Sr from the center toward the edge, which corresponds to the decrease in radial growth rate from center to edge assuming a constant volume rate of precipitation (Figure 5c).

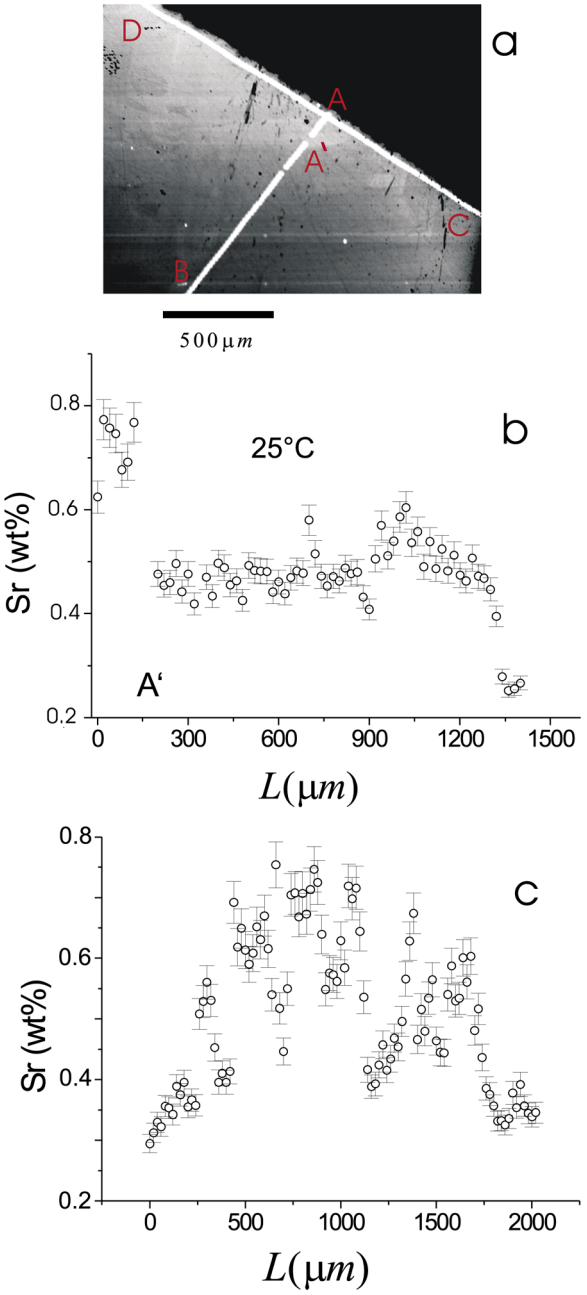

Figure 5. Run D-2. (a) Backscattered electron (BSE) image of polished surface of calcite crystal. Energy Dispersive Spectroscopy showed that the bright spots are particles of Cu or Zn or its compounds, probably introduced from the $CaCl_2 \cdot 6H_2O$ ($5 \cdot 10^{-4}$% of Cu and Zn) we used to prepare solutions. The bright lines indicate the path of the EMP traverse. (b) Electron microprobe profile perpendicular to the crystal/beaker boundary. Error bars (2σ) correspond to the analytical errors from EMP analyses. (c) Electron microprobe profile parallel to the crystal/beaker boundary. Error bars as in Figure 5b.

However, local variations in Sr/Ca are superimposed on this general trend. The composition of the solution was changing during the experiment due to incorporation of Ca and Sr into the growing calcite. The concentrations of Ca and Sr in solution were estimated as a function of time using mass balance (this was straightforward in the case of runs D-1 and D-2, because only one or two crystals were formed). Partition coefficients for each analyzed spot were calculated as $K_d^{Sr} = \frac{(Sr/Ca)_i^{calcite}}{(Sr/Ca)_i^{solution}}$. In this expression, i corresponds to the measured $(Sr/Ca)^{calcite} = f_1(t)$ at a particular spot and $(Sr/Ca)^{solution} = f_2(t)$ at particular point in time related to the amount of calcite grown (see Figure 3). A logarithmic dependence of K_d^{Sr} on growth rate up to a maximum value of ~3 log(nm/s) is presented in Figure 6. The profile across the crystal from run D-1 (Figure 7a) indicated an increase in Sr uptake (Figure 7b) in the light area after passing of point A′. This rapid increase of Sr content in the light area preclude determination of growth rate influence on partitioning; this sharp demarcation could reflect a change in growth mechanism.

[22] In contrast to samples D-1 (2 crystals) and D-2 (1 crystal), runs D-3, D-4, D-5, and D-6 yielded a large number of crystals; hence the assumption of constant volumetric precipitation rate of individual crystals may not be valid. Moreover, crystals of small sizes (80–200 μm) were too small to gauge

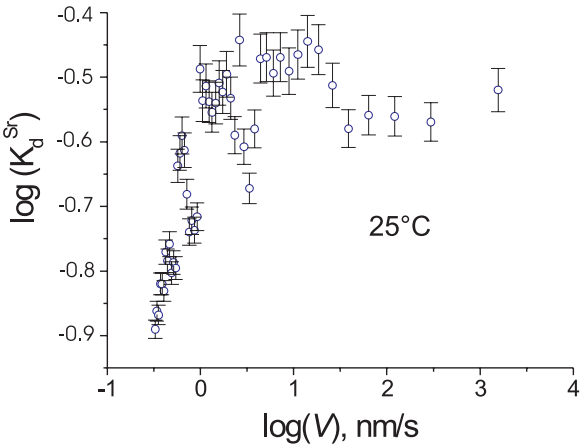

Figure 6. Logarithmic plot of the dependence of Sr partitioning between calcite and solution versus radial growth rate (run D-2, profile parallel to the crystal/beaker boundary). $K_d^{Sr} = \frac{(Sr/Ca)_i^{calcite}}{(Sr/Ca)_i^{solution}}$. 2σ bars were calculated from analytical errors of EMP analyses.

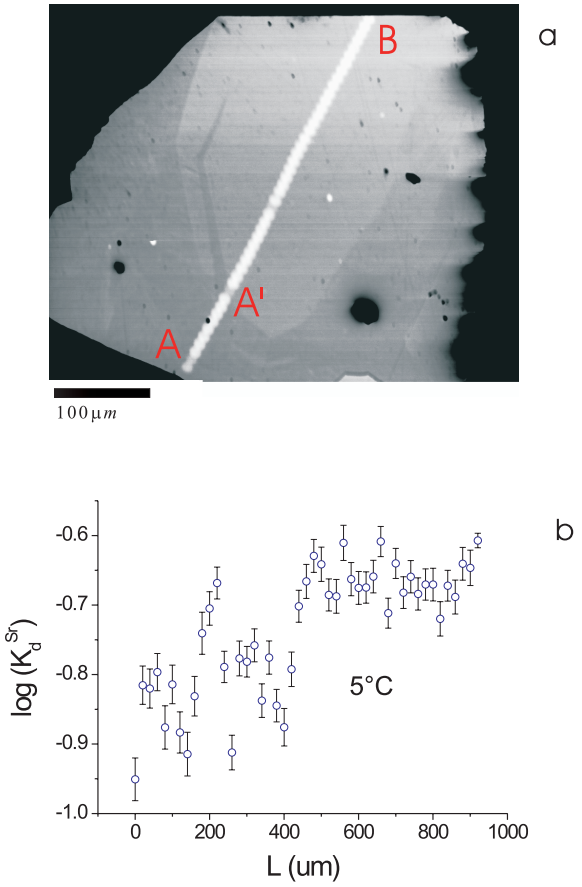

Figure 7. Run D-1. (a) BE image of calcite crystal. The bright line reveals EMP traverse. (b) Sr partitioning into calcite versus distance from the crystal/beaker boundary. Error bars as in Figure 6.

partitioning dependence on growth rate. For this reason, the data from this run are not included in the growth rate plot (Figure 8). However, the minimum K_d^{Sr} values from these experiments are presented on the temperature plot (Figure 9), and the ranges of the partition coefficients are indicated in Table 3. Atomic absorption analyses of run D-3 showed that almost all Ca was consumed by crystallization of calcite from solution. This fact may mask any kinetic effect on Sr uptake in calcite. To examine the influence of solution composition on Sr partitioning we performed two identical experiments D-5 and D-6 where calcite was grown from NH_4-$CaCl_2$ and NaCl-$CaCl_2$ solutions respectively (Tables 1 and 3). The values of K_d^{Sr} from these runs overlap one another because of the relatively large errors of 0.04. Therefore we were unable to definitively evaluate a possible solution composition effect on Sr uptake in calcite other than to conclude that no effect is discernible given the analytical resolution.

[23] Runs at lower ionic strength (I = 0.080) yielded a larger number of crystals relative to the runs at higher ionic strength (I = 0.515). The crystal sizes at low-I were ranging from 60 to 200 μm (most of them were smaller than 100 μm) at 5–55°C. It does suggest that nucleation took place over an extended period during the part of experiment. Therefore we could not determine the growth rate of the crystals from low-I runs. Moreover, it was necessary to mount the crystals in epoxy in random orientations because of their small size, which also precluded accurate determination of analyzed section position relative to the crystal center where nucleation started. The values of K_d^{Sr} determined from these runs varied from 0.11 to 0.39.

3.1. Comparison With Previous Studies

[24] According to the *Watson and Liang* [1995] model we can expect two intervals where K_d is independent on growth rate: (1) $K_d = K_d^{lattice}$ at slow growth where diffusion in the near-surface layer is sufficiently fast to preclude disequilibrium; (2) $K_d^{lattice} = K_d^{surface}$ at fast growth where rapid growth prevents diffusive equilibration. Here

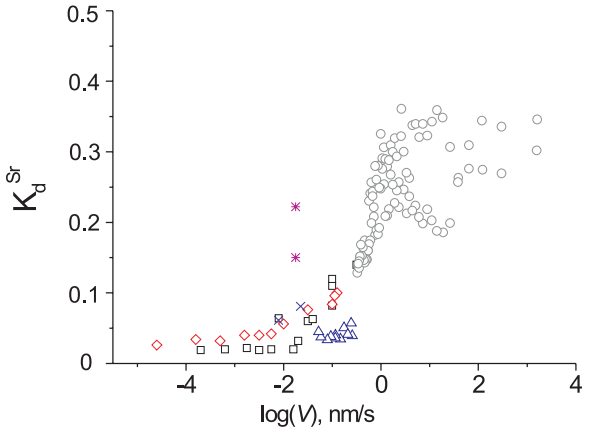

Figure 8. Dependence of Sr partitioning on growth/precipitation rate: Comparison with previous studies. Our data from run D-2 (circles) continue the trends defined by the data of *Lorens* [1981] (diamonds) and *Tesoriero and Pankow* [1996] (squares), confirming the positive dependence of Sr partitioning on calcite growth/precipitation rate. Error bars for run D-2 are the same as in Figure 6. The values of K_d from run C-1 (triangles) are lower than those from *Mucci and Morse* [1983] (stars) and *Huang and Fairchild* [2001] (crosses). The size of the error bars is similar to the symbol size of run C-1.

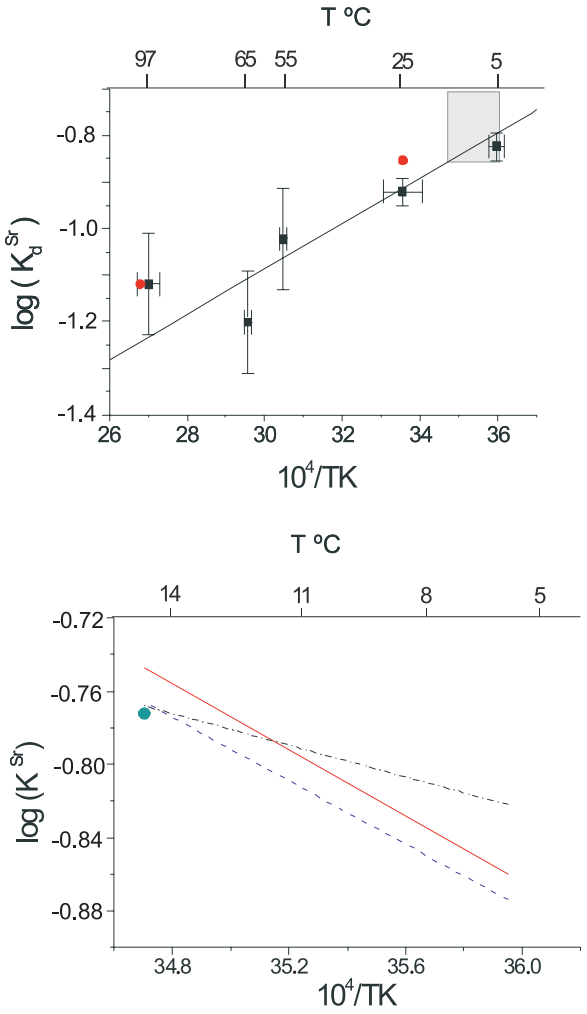

Figure 9. Dependence of minimum K_d^{Sr} on temperature: (top) inorganic calcite and (bottom) foraminiferal calcite. (top) $\Delta H^0 = -9.34 \pm 1.93$ kJ/mol. The circles and squares correspond to the data from *Holland et al.* [1964] and this study. The value of ΔH^0 may be applied for calcite-seawater systems with corrections for Ca and Sr activity coefficients. The second approximation of the Debye-Huckel equation gives similar activity coefficients for both elements of 0.21 in our experimental solutions and 0.19 in seawater at 25°C. In runs D-1 and D-2 at 5 and 25°C changes in the solution composition with time from their large calcite crystals, unlike other runs at higher temperature. Therefore the large error bars in other runs correspond to the total changes of Sr/Ca between initial and final solutions from run D-1. (bottom) Region of gray square from top plot. Calibration data of *Elderfield et al.* [2000] for three different foraminifera species: *hirsuta* (solid line, $r^2 = 0.77$), *truncatulinoides* (dashed line, $r^2 = 0.80$), and *inflata* (dashed and dotted line, $r^2 = 0.65$). The circle is from *Delaney et al.* [1985].

$K_d^{lattice}$ and $K_d^{surface}$ are the equilibrium partition coefficients for the bulk crystal (lattice) and the near-surface layer respectively.

[25] Our results are presented in Figure 8, where the molar precipitation rates from previous studies were converted into linear growth rates in a manner used by *Huang and Fairchild* [2001] and *Watson* [2004]. The data of *Tesoriero and Pankow* [1996] suggested that at $\log V < -2$ Sr partitioning may achieve equilibrium ($K_d^{Sr} = 0.02$). K_d^{Sr} rises rapidly over the growth rate interval $\log V = -1.5 - 0.5$. *Tesoriero and Pankow* [1996] did not determine K_d^{Sr} at higher growth rates. K_d^{Sr} may approach $K_d^{Sr(surface)}$ when $\log V > 2$, where partition coefficient is independent on growth rate (run D-2). Our range of growth rates (0.03 nm/s – 3.16 μm/s) cover those observed for scallop shell calcite (0.23–2.55 nm/s) by *Owen et al.* [2002]. *Dreybrodt* [1996], however, evaluated much smaller rates for speleothems ($3 \cdot 10^{-4}$–0.77 nm/s). Our data from run C-1 are consistent with the data of *Tesoriero and Pankow* [1996]; however, the data of *Huang and Fairchild* [2001], and especially those of *Mucci and Morse* [1983], are substantially higher. *Pingitore and Eastman* [1986] reported that 0.48 M NaCl solutions generate much lower partition values than diluted NaCl-free solutions. The solutions of *Huang and Fairchild* [2001] are diluted by three orders of magnitude relative to other experiments presented in Figure 8. This fact may explain why they observed higher K_d values than we did in similar (cave-type) experiment. *Mucci and Morse* [1983], using Mg-doped solutions, found that Mg enhances K_d^{Sr} up to 50% with increasing Mg/Ca in solution from 1.0 to 5.13. The high values of K_d^{Sr} can also be explained by precipitation of a Sr-rich phase within calcite. In our experiments we eliminated this possibility by performing EMP analyses instead of relying on the bulk analytical technique. To estimate surface enrichment factor F we used K_d^{Sr} values at high growth rates, where 100% entrapment might occur, i.e., $K_d^{Sr} = 0.35$ approaching $K_d^{Sr(surface)}$ (run D-2). We inferred that low Sr partitioning data of *Tesoriero and Pankow* [1996] approaches an equilibrium ($K_d^{Sr} = 0.02$; see Figure 8). The surface enrichment factor can then be estimated as $F = \left[K_d^{Sr(surface)}\right] / \left[K_d^{Sr(lattice)}\right] = 0.35/0.02 = 17.5$.

3.2. Dependence of K_d^{Sr} on Temperature

[26] On the basis of our data and previous studies, Sr uptake in calcite increases with increasing growth rate, so the lowest values of K_d^{Sr} are closer

to the equilibrium case. Therefore we used the minimum K_d^{Sr} values in the $\log K_d^{Sr}$ versus $10^4/T(K)$ plot (Figure 9). The linear fit to our data yields a slope of 0.0488 ± 0.0101 ($r^2 = 0.793$). The enthalpy (ΔH^0) of reaction

$$Sr^{2+}_{(aq)} + CaCO_{3(cr)} = Ca^{2+}_{(aq)} + SrCO_{3(cr)} \quad (2)$$

was determined from the slope of the linear fit: $\Delta H^0 = -slope \cdot RT = -9.34 \pm 1.93$. kJ/mol, where universal gas constant R = 8.3144 J/(mol·K) and T = 298.15K (Figure 9, top). The error was determined from the fitting results ($r^2 = 0.793$). The resulting ΔH^0 value covers those calculated from reaction (2) as $\Delta H^0 = H^0_{product} - H^0_{reagent} = -10.3$ kJ/mol at 298.15K (thermodynamic data are from *Dean* [1999]). This fact suggests that our minimum values of K_d^{Sr} values may approach equilibrium partitioning. However, modeling results (based on the classical molecular dynamics simulations) of *de Leeuw* [2002] yielded $\Delta H^0 = -5.8$ kJ/mol at 298.15K. The slope of the line connecting the data points of *Katz et al.* [1972, Figure 5] is almost the same as ours. At 97–100°C the data are similar to those of *Holland et al.* [1964]. The region of Sr/Ca calibration in planktonic foraminifera is marked as gray area on the top plot. The actual calibrations for three different species are shown on the bottom plot of Figure 9 [*Elderfield et al.*, 2000]. The seawater Sr/Ca ratio of $8.52 \cdot 10^{-3}$ was used in this study. Their partitioning values are similar to ours at 5°C but increase toward 15°C, showing the opposite temperature dependence then our data. This fact may indicate that the Sr/Ca calibration of *Elderfield et al.* [2000] represents disequilibrium growth partitioning. In most cases, biological mineralization occurs in a semiclosed system, i.e., organisms build their shells from the internal calcifying fluid by pumping or diffusion of the elements through a membrane. The composition of this calcifying fluid remains unknown and may be different from seawater. Another possible explanation for the partitioning trend observing by *Elderfield et al.* [2000] is the calcifying fluid may be enriched in Sr relative to seawater. If increasing of the temperature enhances the pumping rate through the membrane then Sr concentration increases in both the calcifying fluid and in the calcite skeleton.

4. Conclusions

[27] Increasing crystal growth rate enhances Sr^{2+} uptake in calcite, suggesting that Sr is probably enriched in the calcite near-surface region relative to the bulk crystal during crystal growth. The value of K_d^{Sr} may approach $K_d^{Sr(surface)}$ when the growth rate exceed 10 nm/s or 31.54 cm/yr. Growth rates slower than $1.6 \cdot 10^{-2}$ nm/s or 0.5 mm/yr are required to reach an equilibrium partitioning of Sr at ambient conditions.

Acknowledgments

[28] We would like to thank Henry Ehrlich, Dave Wark, Kiera Becker, and Damon Chaky for their assistance with atomic absorption, electron microprobe, and gas chromatography analyses at RPI. We thank Patricia Dove and Jeanne Paquette for their helpful review of this manuscript. This work was supported by the National Science Foundation through grants EAR-9804794 and EAR-0337481 to E. B. Watson.

References

Allison, N., and W. E. N. Austin (2003), The potential of ion microprobe analysis in detecting geochemical variations across individual foraminifera tests, *Geochem. Geophys. Geosyst.*, *4*(2), 8403, doi:10.1029/2002GC000430.

Andreasen, G. H., and M. L. Delaney (2000), Bulk calcite size fraction distribution and Sr/Ca composition for deep-sea sediments at selected age horizons, *Mar. Geol.*, *169*, 185–2005.

Cherniak, D. J. (1997), An experimental study of strontium and lead diffusion in calcite, and implications for carbonate diagenesis and metamorphism, *Geochim. Cosmochim. Acta*, *61*, 4173–4179.

Davis, K. J., P. M. Dove, L. E. Wasylenki, and J. J. De Yoreo (2004), Morphological consequences of differential Mg^{2+} incorporation at structurally distinct steps on calcite, *Am. Mineral.*, *89*, 714–720.

de Leeuw, N. H. (2002), Molecular dynamic simulations of the growth inhibiting effect of Fe^{2+}, Mg^{2+}, Cd^{2+}, and Sr^{2+} on calcite crystal growth, *J. Phys. Chem. B*, *106*, 5241–5249.

Dean, J. A. (Ed.) (1999), *Lange's Handbook of Chemistry*, McGraw-Hill, New York.

Delaney, M. L., A. W. H. Be, and E. A. Boyle (1985), Li, Sr, Mg, and Na in foraminiferal calcite shells from laboratory cultural sediment traps, and sediment cores, *Geochim. Cosmochim. Acta*, *49*, 1327–1341.

Dreybrodt, W. (1996), Chemical kinetics, speleothem growth and climate, *Boreas*, *28*, 347–356.

Elderfield, H., C. J. Bertram, and J. Erez (1996), A biomineralization model for the incorporation of trace elements into foraminiferal calcium carbonate, *Earth Planet. Sci. Lett.*, *142*, 409–423.

Elderfield, H., M. Cooper, and G. Ganssen (2000), Sr/Ca in multiple species of planktonic foraminifera: Implications for reconstructions of seawater Sr/Ca, *Geochem. Geophys. Geosyst.*, *1*(11), doi:10.1029/1999GC000031.

Elderfield, H., M. Vautravers, and M. Cooper (2002), The relationship between shell size and Mg/Ca, Sr/Ca, $\delta^{18}O$, and $\delta^{13}C$ of species of planktonic foraminifera, *Geochem. Geophys. Geosyst.*, *3*(8), 1052, doi:10.1029/2001GC000194.

Gabitov, R. I., and E. B. Watson (2004), Experimental study of Sr partition into calcite at various linear growth rates and temperatures: Preliminary results, *Eos Trans. AGU*, *85*(17), Jt. Assem. Suppl., Abstract V43A-05.

Gruzensky, P. M. (1967), Growth of calcite crystals, *J. Phys. Chem. Solids*, *S1*, 365–367.

Holland, H. D., H. J. Holland, and J. L. Munoz (1964), The coprecipitation of cations with $CaCO_3$–II. The coprecipitation of Sr with calcite between 90 and 100°C, *Geochim. Cosmochim. Acta*, *28*, 1287–1301.

Huang, Y., and I. J. Fairchild (2001), Partition of Sr^{2+} and Mg^{2+} into calcite under karst-analogue experimental conditions, *Geochim. Cosmochim. Acta*, *65*, 47–62.

Katz, A., E. Sass, and A. Starinsky (1972), Strontium behavior in the aragonite-calcite transformation: An experimental study at 40–98°C, *Geochim. Cosmochim. Acta*, *36*, 481–496.

Lea, D. W., T. A. Mashiotta, and H. J. Spero (1999), Control of magnesium and strontium uptake in planktonic foraminifera determined by live culturing, *Geochim. Cosmochim. Acta*, *63*, 2369–2379.

Lemarchand, D., G. L. Wasserburg, and D. A. Papanastassiou (2004), Rate-controlled calcium isotope fractionation in synthetic calcite, *Geochim. Cosmochim. Acta*, *68*, 4665–4678.

Lorens, R. B. (1981), Sr, Cd, Mn, and Co distribution coefficients in calcite as a function of calcite precipitation rate, *Geochim. Cosmochim. Acta*, *45*, 553–561.

Lorens, R. B., and M. L. Bender (1980), The impact of solution chemistry on *Mytilus edulis* calcite and aragonite, *Geochim. Cosmochim. Acta*, *44*, 1265–1278.

Martin, P. A., D. W. Lea, T. A. Mashiotta, T. Papenfuss, and M. Sarnthein (1999), Variation of foraminiferal Sr/Ca over Quaternary glacial-interglacial cycles: Evidence for changes in mean ocean Sr/Ca?, *Geochem. Geophys. Geosyst.*, *1*(1), doi:10.1029/1999GC000006.

Mucci, A., and J. W. Morse (1983), The incorporation of Mg^{2+} and Sr^{2+} into calcite overgrowths: Influences of growth rate and solution composition, *Geochim. Cosmochim. Acta*, *47*, 217–233.

Owen, R., H. Kennedy, and C. Richardson (2002), Isotopic partitioning between scallop shell calcite and seawater: Effect of shell growth rate, *Geochim. Cosmochim. Acta*, *66*, 1727–1737.

Paquette, J., and R. J. Reeder (1995), Relationship between surface structure, growth mechanism, and trace element incorporation in calcite, *Geochim. Cosmochim. Acta*, *59*, 735–749.

Parkman, R. H., J. M. Charnock, F. R. Livens, and D. J. Vaughan (1998), A study of the interaction of strontium ions with the surface of calcite and kaolinite, *Geochim. Cosmochim. Acta*, *62*, 1481–1492.

Pingitore, N. E., Jr., and M. P. Eastman (1986), The coprecipitation of Sr^{2+} with calcite at 25 °C and 1 atm, *Geochim. Cosmochim. Acta*, *50*, 2195–2203.

Reeder, R. J. (1996), Interaction of divalent cobalt, zinc, cadmium, and barium with the calcite surface during layer growth, *Geochim. Cosmochim. Acta*, *60*, 1543–1552.

Stipp, S. L., M. F. Hochella Jr., G. A. Parks, and J. O. Leckie (1992), Cd^{2+} uptake by calcite, solid-state diffusion, and the formation of solid-solution: Interface process observed with near-surface sensitive techniques (XPS, LEED, and AES), *Geochim. Cosmochim. Acta*, *56*, 1941–1954.

Stoll, H. M., and D. P. Schrag (2000), Coccolith Sr/Ca as a new indicator of coccolithophorid calcification and growth rate, *Geochem. Geophys. Geosyst.*, *1*(5), doi:10.1029/1999GC000015.

Stoll, H. M., C. Klaas, I. Probert, J. R. Encinar, and J. I. Garcia Alonso (2002a), Calcification rate and temperature effects on Sr partitioning in coccoliths of multiple species of coccolithophorids in culture, *Global Planet. Change*, *34*, 153–171.

Stoll, H. M., Y. Rosenthal, and P. Falkowski (2002b), Climate proxies from Sr/Ca of coccolith: Calibration from continuous culture of *Emiliania huxleyi*, *Geochim. Cosmochim. Acta*, *66*, 927–936.

Tesoriero, A. J., and J. F. Pankow (1996), Solid solution partition of Sr^{2+}, Ba^{2+}, and Cd^{2+} to calcite, *Geochim. Cosmochim. Acta*, *60*, 1053–1063.

Wasylenki, L. E., P. M. Dove, D. S. Wilson, and J. J. De Yoreo (2005a), Nanoscale effects of strontium on calcite growth: An in situ AFM study in the absence of vital effects, *Geochim. Cosmochim. Acta*, *69*, 3017–3027.

Wasylenki, L. E., P. M. Dove, and J. J. De Yoreo (2005b), Effects of temperature and transport conditions on calcite growth in the presence of Mg^{2+}: Implications for paleothermometry, *Geochim. Cosmochim. Acta*, *69*, 4227–4236.

Watson, E. B. (1996), Surface enrichment and trace-element uptake during crystal growth, *Geochim. Cosmochim. Acta*, *60*, 5013–5020.

Watson, E. B. (2004), A conceptual model for near-surface kinetic controls on the trace-element and stable isotope composition of abiogenic calcite crystals, *Geochim. Cosmochim. Acta*, *68*, 1473–1488.

Watson, E. B., and Y. Liang (1995), A simple model for sector zoning in slowly growing crystals: Implications for growth rate and lattice diffusion, with emphasis on accessory minerals in crustal rocks, *Am. Mineral.*, *80*, 1179–1187.